Optics Communications 284 (2011) 3581–3589

Contents lists available at ScienceDirect

Optics Communications

journal homepage: www.elsevier.com/locate/optcom

Photonic microwave generation and transmission using direct modulation of stably injection-locked semiconductor lasers

Sheng-Kwang Hwang [a,d,*], Sze-Chun Chan [b], Shie-Chin Hsieh [a], Cheng-Yu Li [c]

[a] Department of Electro-Optical Engineering, National Cheng Kung University, Tainan, Taiwan
[b] Department of Electronic Engineering, City University of Hong Kong, Hong Kong, China
[c] Graduate Institute of Opto-Mechatronics, National Chung Cheng University, Chia-Yi, Taiwan
[d] Advanced Optoelectronic Technology Center, National Cheng Kung University, Tainan, Taiwan

ARTICLE INFO

Article history:
Received 4 November 2010
Received in revised form 24 March 2011
Accepted 24 March 2011
Available online 12 April 2011

Keywords:
Semiconductor laser
Injection locking
Optical communications
Microwave photonics
Radio-over-fiber
Direct modulation

ABSTRACT

Direct modulation of a semiconductor laser subject to stable injection locking is capable of generating microwave subcarriers that are broadly frequency-tunable, more than 4 times its free-running relaxation resonance frequency, and are highly sideband-asymmetric, more than 22 dB. The latter characteristic makes the laser system particularly attractive for radio-over-fiber applications. Therefore, such modulation sideband asymmetry, its underlying mechanism, and its effect on chromatic dispersion-induced microwave power variation are extensively studied, in particular, over a broad range of injection conditions. Mappings showing integrated and global understandings of the modulation sideband asymmetry together with the modulation frequency enhancement are obtained accordingly. Interestingly, it is found that the microwave frequency can be tuned over a broad range while keeping a similar level of modulation sideband asymmetry and vice versa, either of which is achieved by simply changing the injection condition. This, therefore, considerably adds the flexibility and re-configurability to the laser system. The cavity resonance shift due to injection locking is responsible for not only the enhanced modulation frequency but also the modulation sideband asymmetry, where a modification in its previous interpretation is obtained for explanation. The modified modulation characteristics are strong functions of the linewidth enhancement factor, making it possible to choose lasers with proper values of the factor for different photonic microwave characteristics.

1. Introduction

Microwave photonics has attracted great attention over the past years [1]. This is particularly due to the strong demand in distributing microwave subcarriers over long distances through fibers for broadband wireless access networks [2,3]. Such radio-over-fiber systems adopt an architecture where microwave subcarriers are generated in the optical domain at a central office and next transmitted to remote base stations through fibers. Microwave subcarriers are converted to the electrical domain at the base stations using photodetectors, which are next radiated by antennas over small areas. Therefore, certain characteristics of such generated microwave subcarriers are necessary to simultaneously satisfy the requirements in both the optical domain and the electrical domain. They include high microwave frequency, low phase noise, broadband frequency tunability, and optical single-sideband (SSB) modulation [1,4]. A variety of different schemes have therefore been proposed to simultaneously achieve these photonic microwave characteristics [5–12].

Direct modulation of a semiconductor laser is the simplest scheme for photonic microwave generation and transmission. However, the highest relaxation resonance frequency experimentally demonstrated so far is only around 25 GHz, limiting the highest frequency and the tunable range of the generated microwave subcarriers [13,14]. Besides, the spectral signature of the relaxation resonance is symmetric, suggesting optical double-sideband (DSB) modulation characteristic [15,16]. These inherent properties of the laser make the direct modulation scheme difficult to achieve the above-mentioned photonic microwave characteristics. Operating the laser under stable injection locking by introducing an external optical field, however, offers an attractive solution. Based on a linearized analysis [17], the relaxation resonance of the laser can be radically modified due to stable injection locking, predicting considerable enhancement in relaxation resonance frequency and strong asymmetry in direct modulation sidebands. More than 3-fold enhancement in relaxation resonance frequency has been experimentally observed in a number of different lasers [18–22], demonstrating that direct modulation of a stably injection-locked laser is feasible for very high frequency and broadband tunable microwave generation. The shift of the cavity resonance due to optical injection has been proposed to be responsible for such an enhancement [17,23–26]. Optical SSB modulation

* Corresponding author. Tel.: +886 6 2757575x63922; fax: +886 6 2095040.
E-mail address: skhwang@mail.ncku.edu.tw (S.-K. Hwang).

0030-4018/$ – see front matter © 2011 Elsevier B.V. All rights reserved.
doi:10.1016/j.optcom.2011.03.066

characteristic was observed in recent experiments [27–31], where modulation sideband asymmetry of up to 21.4 dB was found. This characteristic makes direct modulation of a stably injection-locked laser even more attractive for applications where fiber transmission of microwave subcarriers to remote areas is necessary.

As noted, while studies on direct modulation of a stably injection-locked laser have focused mainly on the enhanced relaxation resonance frequency and its underlying mechanism, there have been few or no discussions on the modulation sideband asymmetry, its underlying mechanism, and its effect on dispersion-induced microwave power variation. Particularly, how they behave over a broad range of injection conditions and key laser parameters have not yet been addressed. These discussions are important as they help to better understand the laser system from a global viewpoint and in determining whether the laser system is practically useful. Therefore, the main purpose of this work is to numerically study these issues based on a set of coupled, nonlinear rate equations for the stably injection-locked laser [17,32]. The laser intrinsic noise is considered in the numerical calculation as a broadband optical probe. The corresponding noise spectra not only reveal how the stably injection-locked laser would response to direct modulation [13,18], but also help to study the underlying mechanisms leading to the modified modulation characteristics. Even though the enhanced relaxation resonance frequency of the laser system has been extensively investigated, it is again discussed here briefly to obtain an integrated picture of the overall photonic microwave characteristics of the laser system with our understanding of its modulation sideband asymmetry. While it is not the focus of this study, an interesting phenomenon is observed accordingly, that is, reduction, not enhancement, in the relaxation resonance frequency is found over a range of operating conditions. Such reduction has actually been both experimentally observed [17,18] and numerically verified [25,33] but has not been much emphasized. This, however, stimulates us to revisit the previously proposed underlying mechanism, resulting in the modification of its interpretation.

2. Theoretical model

The optical injection system consists of one master laser and one slave laser, as shown in Fig. 1. The output of the former is directed to the latter using a free-space circulator arrangement that consists of two half-wave plates, one polarizing beam splitter, and one Faraday rotator [34,35]. Additionally, optical isolators can be used to increase the extent of isolation. For a fiber-based system, such an arrangement can be replaced simply by a fiber circulator. The output of the slave laser is sent to a detection system to obtain both optical and microwave spectra. Depending on the level and frequency of the injection from the master laser, the slave laser can undergo a variety of different dynamical states [32,35–38], such as stable injection locking, periodic oscillations, and chaos. For our interest in this study, the laser system is operated under stable injection locking. For photonic microwave generation, the stably injection-locked slave laser is directly modulated by a microwave signal at the required frequency. For photonic microwave transmission, the output of the directly modulated, stably injection-locked slave laser is sent through fibers, where the chromatic dispersion effect on microwave power is investigated.

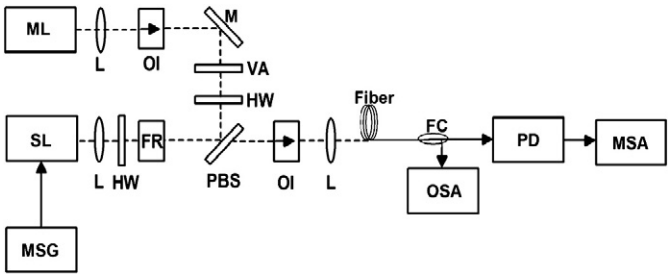

Fig. 1. Schematic of the laser system. ML: master laser; SL: slave laser; L: lens; PBS: polarizing beam splitter; M: mirror; HW: half-wave plate; FR: Faraday rotator; VA: variable attenuator; OI: optical isolator; FC: fiber coupler; PD: photodiode; OSA: optical spectrum analyzer; MSA: microwave spectrum analyzer; MSG: microwave signal generator.

The laser system can be characterized by the following rate equations of a single-mode semiconductor laser subject to both optical injection and direct modulation [17,32]:

$$\frac{dA}{dt} = -\frac{\gamma_c}{2}A + i(\omega_0-\omega_c)A + \frac{\Gamma}{2}(1-ib)gA + \eta A_i e^{-i\Omega t} + F_{sp} \quad (1)$$

$$\frac{dN}{dt} = \frac{J+J_m\,cos(\Omega_m t)}{ed} - \gamma_s N - gS. \quad (2)$$

Here, $A=|A|e^{i\phi}$ is the total complex intracavity field amplitude at the free-running oscillation frequency ω_0, ϕ is the optical phase relative to the injection field, γ_c is the cavity decay rate, ω_c is the angular frequency of the cold cavity, Γ is the confinement factor describing the spatial overlap between the gain medium and the optical mode, b is the linewidth enhancement factor relating the dependence of the refractive index on changes in the optical gain [39], g is the optical gain parameter which is a function of the charge carrier density N and the intracavity photon density S, $F_{sp}=F_r+iF_i$ is the complex field noise characterized by a spontaneous emission rate [40,41], η is the injection coupling rate, A_i is the injection field amplitude, $f=\Omega/2\pi$ is the detuning frequency of the master laser from the free-running frequency of the slave laser, J is the bias current density, J_m is the modulation current density, $f_m=\Omega_m/2\pi$ is the modulation frequency, e is the electron charge, d is the active layer thickness, and γ_s is the spontaneous carrier decay rate. The photon density is related to the field by

$$S = \frac{2\epsilon_0 n^2}{\hbar\omega_0}|A|^2 \quad (3)$$

where ϵ_0 is the free-space permittivity, n is the refractive index, and $\hbar$ is the reduced Plank's constant. Under a steady state, free-running operating condition of the slave laser determined by J, setting Eqs. (1) and (2) equal to zero without considering the field noise, optical injection, and microwave modulation results in $\Gamma g_0=\gamma_c$, $\omega_0-\omega_c=b\gamma_c/2$, and $N_0/S_0=\gamma_c/\Gamma\gamma_s\tilde{J}$, which are used in the following derivations. Note that g_0, S_0, N_0 are the free-running values of g, S, and N, respectively, and $\tilde{J}=(J/ed-\gamma_s N_0)/\gamma_s N_0$ is the normalized bias level above the laser threshold. For the following derivations and discussions, Eq. (1) is further separated into the real and the imaginary part, respectively, as

$$\frac{1}{|A|}\frac{d|A|}{dt} = \frac{1}{2}\Gamma(g-g_0) + \eta\frac{|A_i|}{|A|}\cos(\Omega t+\phi) + \frac{F_r\cos\phi + F_i\sin\phi}{|A|} \quad (4)$$

$$\frac{d\phi}{dt} = -\frac{b}{2}\Gamma(g-g_0) - \eta\frac{|A_i|}{|A|}\sin(\Omega t+\phi) + \frac{F_i\cos\phi - F_r\sin\phi}{|A|} \quad (5)$$

For the purpose of numerical calculation, Eqs. (2), (4), and (5) are recast about the steady-state, free-running operating point of the slave laser, where A and N are normalized to their corresponding free-running values, A_0 and N_0, respectively [32,37]:

$$\frac{da}{dt} = \frac{1}{2}\left[\frac{\gamma_c\gamma_n}{\gamma_s\tilde{J}}\tilde{n} - \gamma_p\left(2a+a^2\right)\right](1+a) + \xi\gamma_c\cos(\Omega t+\phi) + F_a \quad (6)$$

$$\frac{d\phi}{dt} = -\frac{b}{2}\left[\frac{\gamma_c\gamma_n}{\gamma_s\tilde{J}}\tilde{n} - \gamma_p\left(2a+a^2\right)\right] - \frac{\xi\gamma_c}{1+a}\sin(\Omega t+\phi) + \frac{F_\phi}{1+a} \quad (7)$$

$$\frac{d\tilde{n}}{dt} = -\gamma_s \tilde{n} - \gamma_n \tilde{n}(1+a)^2 - \gamma_s \tilde{J}\left(2a+a^2\right) + \frac{\gamma_s\gamma_p}{\gamma_c}\tilde{J}\left(2a+a^2\right)(1+a)^2 + \gamma_s m\left(1+\tilde{J}\right)\cos(\Omega_m t) \quad (8)$$

Here, $a=(|A|/|A_0|-1)$, $\tilde{n}=(N/N_0-1)$, γ_n is the differential carrier decay rate, γ_p is the nonlinear carrier decay rate, F_a and F_ϕ are the normalized field noise, $\xi=\eta|A_i|/\gamma_c|A_0|$ is the normalized strength of the injection field, and m is the microwave modulation strength. In the above derivation, the optical gain is modeled perturbatively about the operating point as

$$g(N,S) = g_0 + \frac{\partial g}{\partial N}(N-N_0) + \frac{\partial g}{\partial S}(S-S_0) = \frac{1}{\Gamma}\left[\gamma_c + \frac{\gamma_c\gamma_n}{\gamma_s\tilde{J}}\tilde{n} - \gamma_p\left(2a+a^2\right)\right] \quad (9)$$

where $\partial g/\partial N=\gamma_n/S_0$ is the differential gain parameter and $\partial g/\partial S=-\gamma_p/\Gamma S_0$ is the nonlinear gain parameter.

The values of the laser parameters adopted in this study were experimentally determined [20], which are $\tilde{J}=1.222$, $\gamma_c=5.36\times10^{11}$ s^{-1}, $\gamma_s=5.96\times10^9$ s^{-1}, $\gamma_p=1.91\times10^{10}$ s^{-1}, $\gamma_n=7.53\times10^9$ s^{-1}, and $b=3$. The corresponding relaxation resonance frequency is given by $(2\pi)^{-1}(\gamma_c\gamma_n+\gamma_s\gamma_p)^{1/2}\approx10.25$ GHz. When direct microwave modulation is applied to the slave laser in the following analyses, m is kept at 0.1 for all operating conditions. A second-order Runge–Kutta method with the measured laser parameters is used to solve Eqs. (6)–(8), which has been demonstrated to reproduce all the experimentally observed phenomena [32,35–37]. Since the validity of the model described above has been verified with experimental data up to $\xi=0.4$ [19], simulation data only up to the same injection level is presented here.

3. Results and analyses

3.1. Dynamical and modulation characteristics

Because of optical injection, the dynamics of the injection-locked slave laser is considerably different from that of the free-running counterpart, leading to their differences in direct modulation characteristics. Therefore, it is important to also study the dynamical characteristics of the slave laser in order to investigate the underlying mechanisms. This is achieved by considering the intrinsic spontaneous emission noise of the slave laser, as shown in Eqs. (6) and (7), in our numerical calculation as a broadband optical probe. Note that the intrinsic noise of the master laser is not taken into account throughout the study, which equivalently assumes a highly coherent optical injection.

For the purpose of comparison, the optical spectrum of the free-running slave laser is first demonstrated in Fig. 2(a) as the black curve, showing that the laser oscillates at the cavity resonance. Relaxation resonance sidebands emerge equally and oppositely away from the laser oscillation [15], which is about 10 GHz for the laser under study. Such a frequency offset is commonly adopted to approximate the relaxation resonance frequency of a laser [16,17] and is denoted as f_r for the same purpose here. Although the lower resonance sideband is slightly stronger due to positive b [16], the sidebands are of comparable intensity. This implies similar resonance enhancement at frequencies either negatively or positively offset from the laser oscillation. Therefore, direct modulation of the free-running slave laser generates modulation sidebands of similar intensity, shown as the blue curve in Fig. 2(a) under $f_m=f_r$, leading to an optical DSB signal.

Optical spectra of the stably injection-locked slave laser under different injection conditions are shown as black curves in Fig. 2(b)–(f). For each condition, the optical injection imposes the slave laser to follow its optical phase and thus to oscillate at the injection frequency instead. The linewidth of the slave laser is greatly reduced due to the highly coherent injection signal. More importantly, the dynamical characteristics of the relaxation resonance are radically modified, which follows a strong and complex dependence on the injection conditions. First, f_r increases linearly and continuously with increasing ξ and f, where up to 4-fold enhancement is observed. This is more clearly demonstrated in Fig. 3(a). Analytically calculated eigenfrequencies based on a linearized model by Simpson et al. [17] are also presented as curves, which agree with numerically obtained f_r based on our nonlinear model. This demonstrates the validity of our calculation. For a more complete understanding, the dependence of f_r on both ξ and f is presented as a mapping in Fig. 4(a). A large region of the stable locking dynamics is identified below the Hopf bifurcation line and above the unlocking boundary. The contour lines of constant f_r reveal that it enhances with both ξ and f in nearly the whole stable locking region. Therefore, direct modulation of the injection-locked slave laser at f_r is capable of generating widely tunable microwave signals of nearly 40 GHz. An even higher f_r can be achieved if ξ and f can be practically increased further [22]. If a higher free-running f_r is given to begin with by using a higher bias level of the same laser [18] or a different laser with higher speed [19,20], a much higher f_r can also be obtained. Note that, however, f_r can also reduce under very weak injection, as shown in Fig. 3(a), and therefore there exists a narrow range of reduced f_r along the unlocking boundary in Fig. 4(a). This not only provides useful

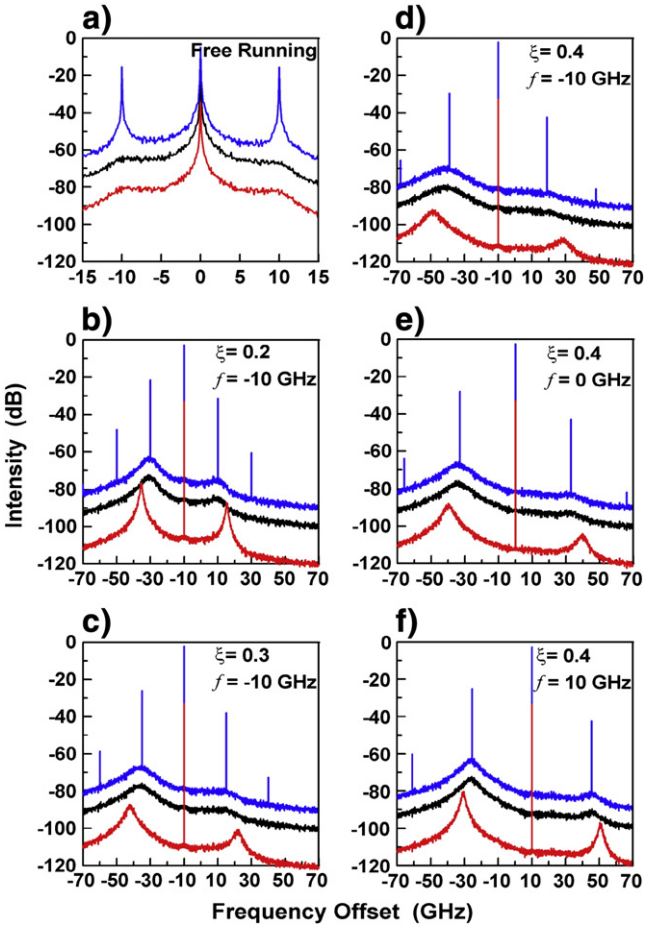

Fig. 2. Optical spectra of the slave laser under different operating conditions, as marked in each plot. Black and blue curves show the spectra without and with direct modulation, respectively, under $b=3$. Red curves show the spectra without direct modulation under $b=7$. For clear visibility, blue curves are up-shifted by 10 dB and red curves are down-shifted by 20 dB from their original values. The frequency axis is relative to the free-running frequency of the slave laser.

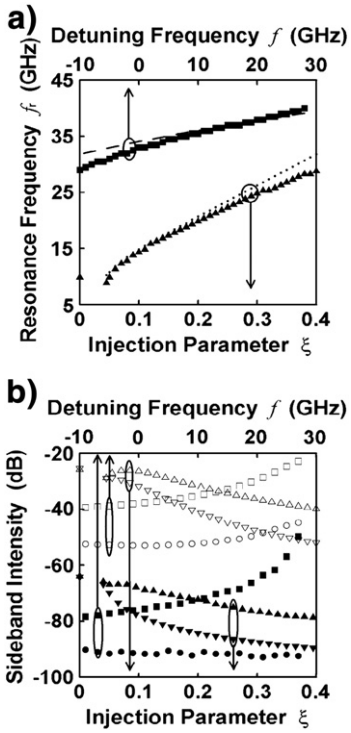

Fig. 3. (a) Resonance frequency in terms of f when $\xi=0.4$ (squares: numerical; dashed curve: analytical), and in terms of ξ when $f=-10$ GHz (triangles: numerical; dotted curve: analytical). The free-running f_r is also presented as a triangle at $\xi=0$. (b) Intensities of resonance sidebands (closed symbols) and modulation sidebands (open symbols) in terms of f when $\xi=0.4$ (squares: lower sidebands; circles: upper sidebands), and in terms of ξ when $f=-10$ GHz (up-triangles: lower sidebands; down-triangles: upper sidebands). The corresponding sidebands of the free-running laser are also presented as up- and down-triangles at $\xi=0$.

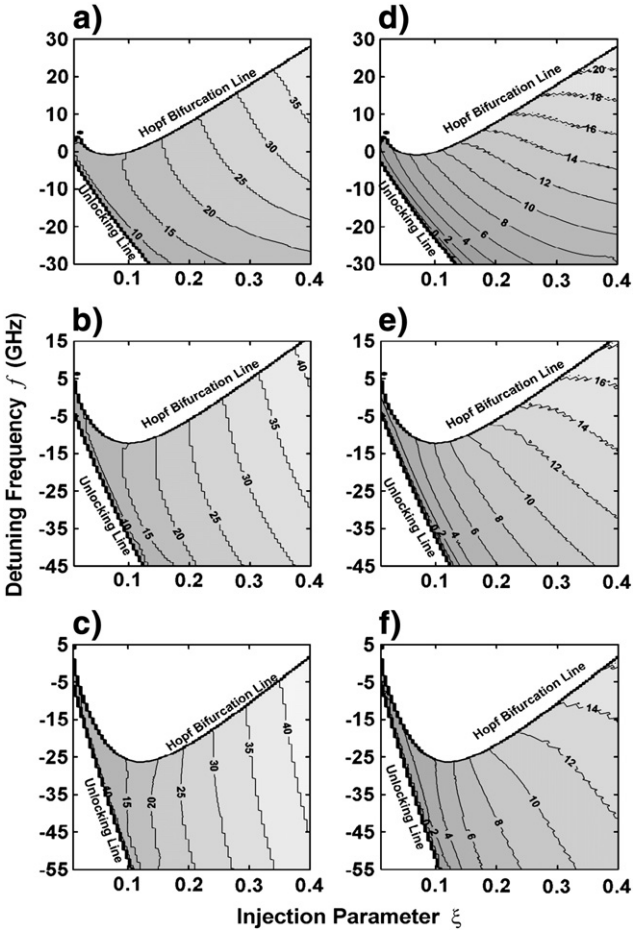

Fig. 4. (a)–(c) Mappings of the resonance frequency as a function of ξ and f for $b=3$, 5, and 7, respectively. Each contour line indicates a constant f_r, as marked, in GHz. (d)–(f) Mappings of the sideband rejection ratio as a function of ξ and f for $b=3$, 5, and 7, respectively. Each contour line indicates a constant R, as marked, in dB.

information in operating the laser system under certain injection conditions for practical applications, but also is used to evaluate the validity of the previously proposed mechanism in explaining this interesting yet to be studied observation. Detailed discussions will be given in Section 3.3.

The modification in the intensities of the resonance sidebands is more complex. Comparing the black curves in Fig. 2(a)–(f), the modified intensity is generally weaker than its free-running value, indicating a suppression of the spontaneous emission noise [18,33]. In addition, it decreases with increasing ξ but with decreasing f. By looking up the operating conditions considered in Fig. 2(b)–(f) in Fig. 4(a), this indicates that the relaxation resonance is highly suppressed for injection conditions away from the Hopf bifurcation line but is largely enhanced at the proximity. It becomes undamped once the Hopf bifurcation line is crossed, leading to the emergence of period-one nonlinear dynamics [12,24,32,35]. Another significant modification is that the lower resonance sideband dominates the upper one, the extent of which increases with increasing ξ and f. These modifications are more clearly demonstrated in Fig. 3(b), where the intensities of both resonance sidebands are presented as closed symbols. These observations suggest that the resonance enhancement is generally stronger at frequencies negatively offset from the laser oscillation. Direct modulation of the injection-locked slave laser, therefore, generates modulation sidebands with asymmetric intensity, shown as blue curves in Fig. 2(b)–(f) under $f_m=f_r$. This is more clearly shown as open symbols in Fig. 3(b). The behavior of either the lower or the upper modulation sideband follows closely with that of the corresponding resonance sideband, respectively. Different extent of such asymmetry in modulation sidebands results in different levels of SSB features and can be quantified by the sideband rejection ratio, R, as the relative strength of the lower modulation sideband to the upper one. The dependence of R on both ξ and f is presented as a mapping in Fig. 4(d) under $f_m=f_r$. Increasingly SSB features with ξ and f are observed as the injection condition moves away from the unlocking boundary, which shows a behavior similar to the enhancement in f_r. Therefore, to simultaneously obtain the highest possible f_r and R of the laser system is feasible. As high as $R\approx 22$ dB is achieved under the range of study. An even higher R can be obtained if ξ and f can be practically increased further. Note that, however, symmetric resonance sidebands and thus modulation sidebands are also observed in Fig. 3(b) for very weak injection, of which intensities are close to those of their free-running counterparts. This implies that $R<0$ dB could happen, which is indeed observed over a very narrow range along the unlocking boundary in Fig. 4(d).

The intensity asymmetry in the modulation sidebands, in fact, depends on modulation frequency, f_m, as shown in Fig. 5(a). By looking up each operating condition considered in Fig. 5(a) in Fig. 4(a), it is observed that each R curve reaches its maximum at f_m which is generally a few gigahertz below the corresponding f_r of each operating condition. The maximum R is, however, only a few decibels higher than that at f_r, which leads to an insignificant difference in microwave power variation between the two modulation conditions, as will be found in Section 3.2. For a further understanding, representative responses of both modulation sidebands in terms of f_m are shown in Fig. 5(b). The strong decrease in the response of the upper modulation sideband with f_m contributes mainly to the increase in R. An inverse of such response leads to a dip at frequencies below f_r. The maximum R thus occurs at a frequency between the dip and f_r.

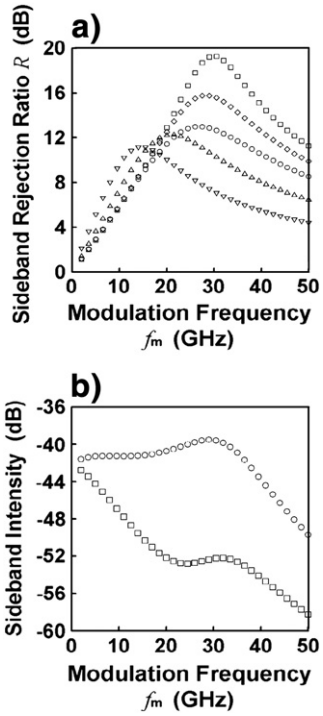

Fig. 5. (a) Sideband rejection ratio in terms of f_m. Squares: $(\xi, f) = (0.4, 10\ \text{GHz})$; diamonds: $(\xi, f) = (0.4, 0\ \text{GHz})$; circles: $(\xi, f) = (0.4, -10\ \text{GHz})$; up-triangles: $(\xi, f) = (0.3, -10\ \text{GHz})$; down-triangles: $(\xi, f) = (0.2, -10\ \text{GHz})$. (b) Responses of the lower (circles) and the upper (squares) modulation sidebands in terms of f_m for $(\xi, f) = (0.4, -10\ \text{GHz})$.

3.2. Chromatic dispersion effect

For a microwave-modulated optical signal, such as the blue curves in Fig. 2, propagating along a fiber, each frequency component experiences a phase shift of [42]

$$\beta(\omega)l \approx \beta(\omega_\lambda)l + \beta'(\omega_\lambda)(\omega-\omega_\lambda)l + \frac{1}{2}\beta''(\omega_\lambda)(\omega-\omega_\lambda)^2 l \tag{10}$$

where β is the propagation constant of the component at the angular frequency ω and is expanded in a Taylor series around the optical carrier frequency ω_λ, β' is the inverse of the group velocity, β'' is the group-velocity dispersion or chromatic dispersion, and l is the transmission distance. While terms higher than the second order are usually not considered due to their insignificance for an optical carrier far away from the zero-dispersion point, the zeroth-order term and the first-order term only introduce a constant phase delay and a constant group delay, respectively, to the modulated optical signal. Therefore, a phase difference existing between frequency components after fiber transmission arises from the second-order term which is more commonly expressed as [42]

$$\theta(\omega) = \frac{-\lambda^2 l D_\lambda}{4\pi c}(\omega-\omega_\lambda)^2 \tag{11}$$

where $\beta'' = -\lambda^2 D_\lambda/2\pi c$ is used, D_λ is the dispersion coefficient at the optical carrier wavelength λ, and c is the speed of light in free space. Hence, at remote base stations, the photodetected beat signals between the modulation sidebands and the optical carrier may add up constructively or destructively depending on their phase relationship described by Eq. (11) where the distance of fiber transmission plays the key role under the same microwave modulation frequency and the same optical carrier wavelength. This gives rise to a fluctuation of the generated microwave power at base stations of different distances [4].

To study the chromatic dispersion effect on the generated microwave power, the laser system is first numerically calculated using Eqs. (6)–(8) to obtain the complex optical spectrum. The frequency-dependent phase shift described in Eq. (11) is then introduced into the spectrum. Note that, as in a typical Corning SMF-28 fiber, $\lambda = 1.55\ \mu\text{m}$ and $D_\lambda = 17$ ps/km-nm are adopted here and no fiber attenuation is considered. The modified optical spectrum is next Fourier-transformed into the time-domain optical field. The field is squared into intensity, which is transformed back to the frequency domain. The result is the power spectrum detected after the propagation through the fiber. Fig. 6(a) shows the generated microwave power as a function of the fiber length for optical signals with different sideband features under $f_m = f_r$. For the free-running slave laser, a deep and repetitive variation of the microwave power is observed due to the DSB feature of the optical signal, resulting in a maximum power variation, ΔP, of a substantially large value, infinity in theory. For the injection-locked slave laser, however, a significantly smaller power variation is experienced due to the non-DSB features of the optical signals. It is observed that ΔP reduces with increasing ξ and f, or equivalently increasing R, indicating the dependence of the immunity to the power variation on different levels of SSB features. To obtain a global understanding, a mapping of ΔP is shown in Fig. 6(b). The immunity to the power fluctuation generally enhances with increasing ξ and f, which is a direct result of SSB features presented in Fig. 4(d). As small as $\Delta P \approx 1$ dB is observed over the range considered here. By comparing Figs. 4(a) and 6(b), the generated microwave signal is broadly tunable between 15 and 40 GHz if $\Delta P = 6$ dB can be tolerated, which is about $R = 9$ dB in Fig. 4(d). In addition, the microwave signal can be tuned over a wide frequency range while maintaining a similar ΔP. On the other hand, different ΔP values can be obtained while keeping a similar microwave frequency. Therefore, by simply changing the injection condition, the laser system can be made flexible and re-configurable for different required photonic microwave characteristics in practical applications.

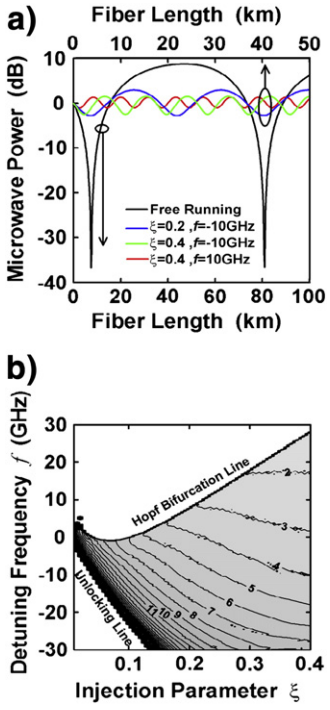

Fig. 6. (a) Microwave power after fiber propagation for operating conditions as marked in the plot, which is normalized to each corresponding value at 0 km. (b) Mapping of the maximum microwave power variation as a function of ξ and f. Each contour line indicates a constant ΔP, as marked, in dB. For contour lines corresponding to $\Delta P \geq 12$ dB, numbers are not marked for clear presentation.

3.3. Cavity resonance shift

As shown in Fig. 2(b)–(f), the optical injection pulls the intracavity field oscillation away from the free-running cavity resonance toward the injection frequency while the optical injection progressively locks the optical phase of the slave laser. Such an injection pulling effect is explained by the Adler's equation which governs the phase dynamics of a general oscillator [43] and is described here by Eq. (5) if only the second term on the right-hand side is considered. However, the introduction of the external field lowers the necessary gain for the slave laser from its free-running value by $\Gamma(g-g_0)$ [17]. This results in the increase of the refractive index of the laser cavity through b, which is known as the antiguidance effect. Accordingly, the cavity resonance is red-shifted from its free-running value by [39]

$$\omega_s = \frac{b}{2}\Gamma(g-g_0) = \frac{b}{2}\left[\frac{\gamma_c\gamma_n}{\gamma_s}\tilde{n} - \gamma_p\left(2a+a^2\right)\right] \tag{12}$$

where Eq. (9) is used to obtain the last expression. Such a red-shifting effect attempts to shift the intracavity field oscillation toward the injection-shifted cavity resonance, which is also involved in the phase dynamics of the laser as described by the first term in Eq. (5). Therefore, a dynamical competition exists between the injection-shifted cavity resonance and injection-imposed laser oscillation, leading to the modification of the laser dynamics.

Stable injection locking occurs when the injection pulling effect dominates. Nevertheless, signals emerging around the red-shifted cavity resonance would be preferably amplified. Therefore, the enhanced f_r reflects the amplification of the relaxation resonance sideband around the shifted cavity resonance, which was proposed by Simpson et al. [17]. This is clearly demonstrated in Fig. 7(a), where the lower resonance sideband frequency, f_l, relative to the free-running slave laser oscillation is obtained with Eqs. (6)–(8) and the shifted cavity resonance frequency, $f_s = \omega_s/2\pi$, is calculated using Eq. (12). In general, the lower resonance sideband emerges lower than the shifted cavity resonance by about 5 to 10 GHz under study. To better demonstrate their relationship, a relative frequency difference is also shown in Fig. 7(a) and is defined as

$$\frac{\Delta f}{f_r} = \frac{f_l - f_s}{f_r}. \tag{13}$$

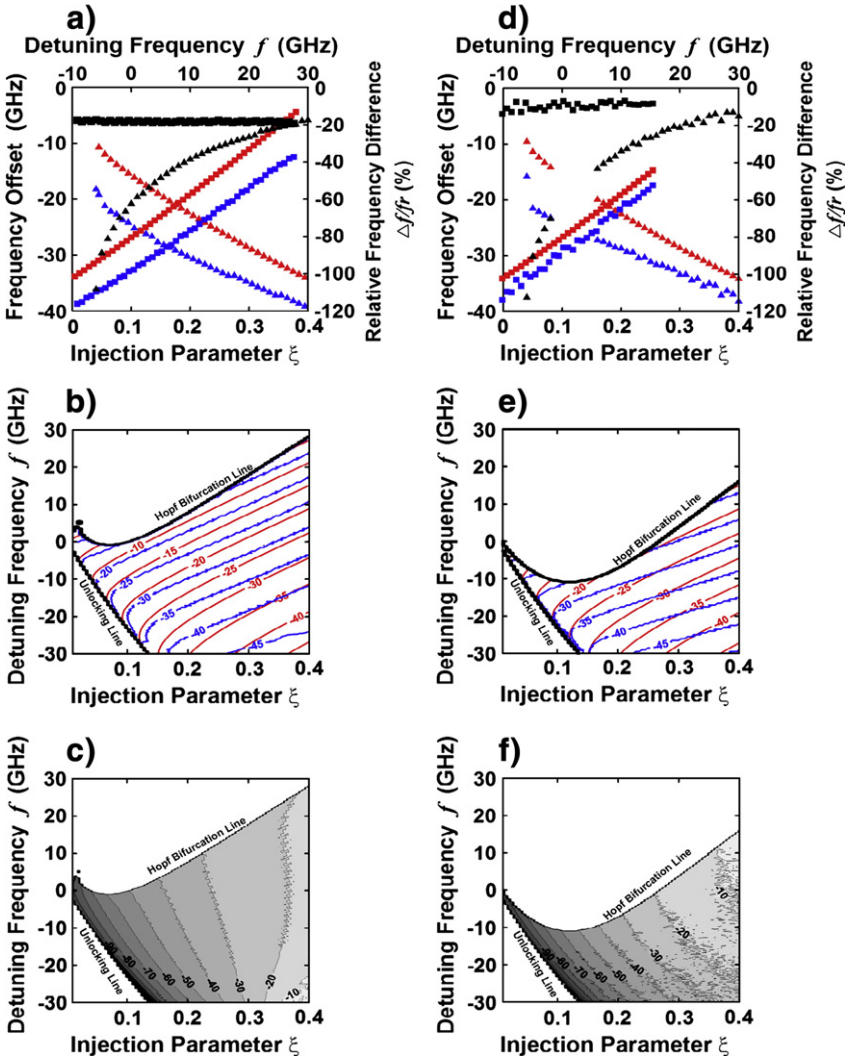

Fig. 7. (a) and (d) The shifted cavity resonance frequency (red symbols), lower resonance sideband frequency (blue symbols), and relative frequency difference (black symbols) in terms of f when $\xi = 0.4$ (squares) and in terms of ξ when $f = -10$ GHz (triangles). (b) and (e) Mappings of the shifted cavity resonance frequency (red curves) and the lower resonance sideband frequency (blue curves) as functions of ξ and f. Each contour line indicates a constant frequency in GHz and is marked by its corresponding number where possible. (c) and (f) Mappings of the relative frequency difference in terms of ξ and f. Each contour line indicates a constant percentage and is marked by its corresponding number, where possible, without the symbol %. The data shown in (a)–(c) is calculated when $\gamma_p = 1.91\times10^{10}$ s^{-1} while (d)–(f) is obtained when $\gamma_p = 0$.

When $-100\% \le \Delta f/f_r \le 0\%$, the shifted cavity resonance appears between the injection-imposed oscillation frequency and the lower resonance sideband frequency. Relatively speaking, the larger the value is, the closer the shifted cavity resonance is to the lower resonance sideband. When $-200\% \le \Delta f/f_r \le -100\%$, however, it appears between the injection-imposed oscillation frequency and the upper resonance sideband frequency. The smaller the value is, the closer the shifted cavity resonance is to the upper resonance sideband. These observations suggest that f_r is largely determined by, but not equal to, the frequency offset between the injection-imposed oscillation and the shifted cavity resonance. They also suggest that the lower resonance sideband and thus the lower modulation sideband would generally receive a stronger resonance enhancement than the upper ones, leading to their dominance shown in Figs. 2–5.

To further explain the observed modifications in relaxation resonance based upon the red-shifting effect, let us study Fig. 7(a) with more details. Under a fixed f of -10 GHz, a stronger optical injection leads to a larger cavity red-shift due to a larger reduction in the required optical gain. The lower resonance sideband thus appears further away from the injection frequency, resulting in a higher f_r shown in Fig. 3(a). However, the slave laser is more strongly locked to the optical injection, resulting in the intensity reduction of resonance sidebands, as shown in Fig. 3(b). For very weak injection, such as $\xi = 0.045$ in Fig. 7(a), the shifted cavity resonance appears very close to the injection-imposed oscillation frequency. This could lead to a similar or even a reduced f_r compared with its free-running value, as shown in Fig. 3(a), since the lower resonance sideband is generally 5 to 10 GHz lower than the shifted cavity resonance under study. In addition, the lower resonance sideband now receives no or little amplification from the shifted cavity resonance and thus appears similarly in intensity to the upper one and to the free-running counterpart, as demonstrated in Fig. 3(b). On the other hand, under a fixed ξ of 0.4, the red-shift of the cavity resonance reduces with increasing f, implying the impact of the injection decreases. Therefore, the lower resonance sideband appears closer to the free-running oscillation frequency. However, the reduction in frequency shift of the lower resonance sideband is relatively small compared to the increment in f, resulting in an increasing f_r with f, as shown in Fig. 3(a). Moreover, the intensities of the resonance sidebands, particularly the lower one, enhance with increasing f since the injection locking effect is weaker, as shown in Fig. 3(b).

For a more complete understanding, the frequency dependence of the shifted cavity resonance and the lower resonance sideband on ξ and f is presented in Fig. 7(b). The red-shifts of the cavity resonance and thus the lower resonance sideband increase with increasing ξ and decreasing f. In general, the lower resonance sideband emerges lower than the shifted cavity resonance by about 5 to 10 GHz under study. There exists a very narrow range along the unlocking boundary where the shifted cavity resonance appears close to or even higher than the injection-imposed oscillation frequency. This is more clearly demonstrated by the relative frequency difference shown in Fig. 7(c) when it is close to or even smaller than -100%. This suggests that the frequency offset between the lower resonance sideband and the injection-imposed oscillation could be smaller than 10 GHz, resulting in the reduced f_r along the boundary shown in Fig. 4(a). This also suggests that the upper resonance sideband and the upper modulation sideband could receive a stronger resonance enhancement instead, leading to $R<0$ dB along the boundary shown in Fig. 4(d).

3.4. Effects of b

As discussed above, the cavity resonance shift plays a key role in the modification of the laser dynamics, which depends strongly on b based on Eq. (12). Note that a and $\tilde{n}$ are coupled with ϕ through optical injection, as shown in Eqs. (6)–(8), and thus they are functions of b as well. This suggests that the cavity resonance shift depends on b much more complicated than it appears in Eq. (12). Therefore, to study the photonic microwave characteristics as functions of b is of great value in the effort to harness the laser system for practical applications. Recall that b describes the dependence of the refractive index on changes in the optical gain. The higher the value of b is, the larger the change of the refractive index becomes. Therefore, under a fixed injection condition, the red-shift of the cavity resonance would increase with b, as demonstrated in Fig. 8(a). However, such b dependence is not linear and is stronger for larger ξ and lower f. A similar behavior of the lower resonance sideband is observed accordingly, where the frequency shift increases more significantly as compared with that of the cavity resonance, suggesting a much stronger function of b. This in turns leads to an increasing f_r with b, which can be clearly observed in Fig. 2 where optical spectra under $b=3$ and 7 are both shown for comparison. As also demonstrated in Fig. 2, the intensities of both resonance sidebands enhance with b, where the enhancement for the lower sideband is stronger than that for the upper one. For the free-running laser, however, Fig. 8(a) shows

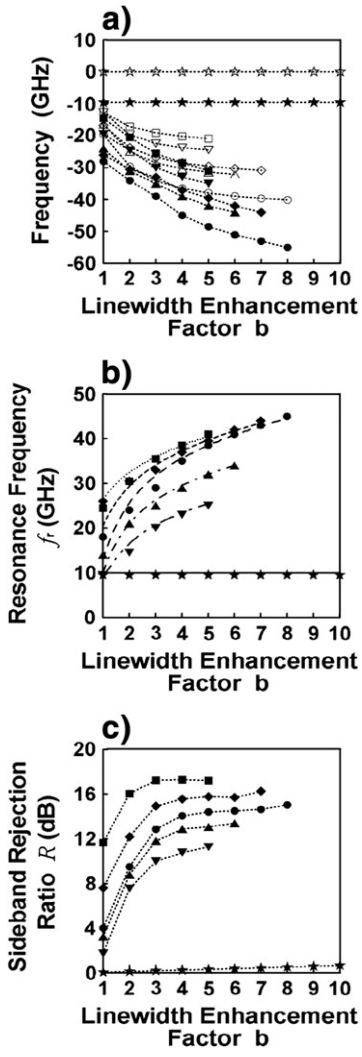

Fig. 8. (a) Frequencies of the shifted cavity resonance (open symbols) and the lower relaxation resonance sideband (closed symbols) with respect to the free-running laser oscillation in terms of b. (b) Resonance frequency in terms of b. (c) Sideband rejection ratio in terms of b under $f_m = f_r$. The same symbols are used for the same operating condition in all three plots as described below. Squares: $(\xi, f) = (0.4, 10\ \text{GHz})$; diamonds: $(\xi, f) = (0.4, 0\ \text{GHz})$; circles: $(\xi, f) = (0.4, -10\ \text{GHz})$; up-triangles: $(\xi, f) = (0.3, -10\ \text{GHz})$; down-triangles: $(\xi, f) = (0.2, -10\ \text{GHz})$; stars: free running. Curves are for clear visibility in (a) and (c) but for analytically calculated eigenfrequencies in (b).

that the cavity resonance and the lower resonance sideband appear unchanged in frequency irrespective of the b value.

The corresponding changes in f_r and R with b are demonstrated in Fig. 8(b) and (c), respectively. While f_r increases monotonically with b, such increment enhances with increasing ξ and decreasing f, which is more apparently observed at small b values and is a result of Figs. 7(a) and 8(a). Analytically calculated eigenfrequencies based on a linearized model [17] are also presented as curves in Fig. 8(b), which are consistent with numerically obtained f_r based on our nonlinear model. On the other hand, R increases strongly with b at small values but weakly at large values. To obtain an overall picture, mappings of f_r and R in terms of ξ and f under different b values are shown in Fig. 4. Since the laser cavity prefers to oscillate at a frequency lower than the free-running laser oscillation under optical injection, the slave laser would likely be locked at negative f values, particularly for weak injection. This leads to the asymmetry of the stable locking region around $f=0$ GHz. The extent of the asymmetry enhances with b since the red-shift of the cavity resonance increases, resulting in a significant shift of the stable locking region toward negatively increasing f. In general, f_r and R increase with b under fixed values of ξ and f. This shall help to choose lasers with proper b values for preferred photonic microwave characteristics if only certain values of ξ and f are practically accessible. Note that the largest achievable R at a given b value, however, decreases with increasing b if the values of ξ and f are all practically accessible. The regions along the unlocking boundary where $f_r<10$ GHz and $R<0$ dB are found to shrink with b, some of which are too small to be clearly observed in the plots.

4. Discussion and conclusion

Before concluding our study, a few remarks on the explanation of f_r enhancement in previous research works are made as follows. Based on the concept proposed by Simpson et al. [17], Murakami et al. [23] developed a model by assuming that the modified f_r equals the frequency offset between the injection-imposed oscillation and the shifted cavity resonance, and also by excluding the nonlinear gain effect which has been verified to play a significant role in laser dynamics [13–17,37]. While their analysis seemed more appropriate for strong ξ and positive f accordingly, they observed that the lower resonance sideband in fact appears lower than the shifted cavity resonance by about 1 GHz, corresponding to a relative frequency difference of about −12%. This was, however, completely ignored in their discussion. To further improve the explanation, Wieczorek et al. [25] suggested that, in addition to the cavity resonance shift, the charge carrier pulsation also plays a key role in the modified relaxation resonance. Based on their analysis, however, such a contribution is negligible to the modification in f_r since the lower resonance sideband emerges almost at the shifted cavity resonance, where a relative frequency difference of −2 to −4% was observed. Therefore, they arrived at the same conclusion by Murakami et al. that the modified f_r equals the frequency offset between the injection-imposed oscillation and the shifted cavity resonance. This is, however, inadequate to completely explain the modification in f_r, particularly its reduction, shown in Figs. 2–4. To clearly demonstrate it, Fig. 7(d)–(f) are obtained under $\gamma_p=0$ for a fair comparison with the works by Murakami et al. and Wieczorek et al. While the lower resonance sideband in Fig. 7(d) and (e) appears higher in frequency than that in Fig. 7(a) and (b), the shifted cavity resonance frequency remains almost unchanged. Nevertheless, their behaviors in terms of ξ and f are found similarly to those discussed above when γ_p is present. For our purpose here, let us simply discuss Fig. 7(d) under $f=-10$ GHz. For example, at $\xi=0.08$, the shifted cavity resonance appears at the frequency offset of −14 GHz, leading to $f_r=4$ GHz based on Murakami et al. and thus suggesting a reduction. However, it should be 13 GHz according to Fig. 7(d), indicating an enhancement instead. Note that the free-running f_r is about 10 GHz when $\gamma_p=0$. More interestingly, at $\xi=0.04$, the shifted cavity resonance appears at the frequency offset of about −10 GHz, resulting in $f_r\approx 0$ GHz based on Murakami et al. and thus implying no relaxation resonance. However, it should be 6 GHz based on Fig. 7(d), showing in fact a reduction. Apparently, the condition set by Murakami et al. and Wieczorek et al. should be relaxed as in our analysis above for a better explanation. The frequency difference between the shifted cavity resonance and the lower resonance sideband results from the injection effect, as observed in Eq. (1). While the first three terms calculate the cavity shift effect, the forth term takes into account the injection effect, both of which are necessary to determine the modified relaxation resonance.

In conclusion, photonic microwave generation and transmission using direct modulation of a semiconductor laser subject to stable injection locking is investigated. The relaxation resonance sidebands of the injection-locked laser are considerably shifted in frequency and asymmetrically modified in intensity. Direct modulation of the laser system is therefore capable of generating microwave subcarriers of high microwave frequency and strong sideband asymmetry, the values of which depend strongly on the injection condition. The latter characteristic is particularly preferable for radio-over-fiber applications. Therefore, such modulation sideband asymmetry, its underlying mechanism, and its effect on chromatic dispersion-induced microwave power variation are extensively studied over a broad range of injection condition through mappings. Integrated and global understandings of both modified modulation characteristics are thus obtained, which shall be of great value for practical applications. For example, the microwave frequency can be tuned over a broad range while keeping a similar level of modulation sideband asymmetry, or different levels of modulation sideband asymmetry can be obtained while keeping a similar microwave frequency, either of which is achieved by simply changing the injection condition. This, therefore, considerably adds the flexibility and re-configurability to the laser system. The cavity resonance shift due to injection locking is responsible for not only the enhanced modulation frequency but also the modulation sideband asymmetry. A modification of its interpretation based on previous research works is, however, necessary to better explain the former. Both modified modulation characteristics depend strongly on the linewidth enhancement factor which plays a key role in the cavity resonance shift. Since the factor depends highly on the gain medium and the laser structure, it is therefore possible to choose lasers with proper values of the factor for different required photonic microwave characteristics in practical applications.

Acknowledgements

S.K. Hwang's work is fully supported by the National Science Council of Taiwan under Contract No. NSC97-2112-M-006-012-MY2 and NSC99-2112-M-006-013-MY3, and S.C. Chan's work is fully supported by a grant from City University of Hong Kong under Project No. 7008046 and a grant from the Research Grants Council of Hong Kong, China under Project No. CityU 111308.

References

[1] J.P. Yao, J. Lightwave Technol. 27 (2009) 314.
[2] H. Ogawa, D. Polifko, S. Banba, IEEE Trans. Microwave Theory Tech. 40 (1992) 2285.
[3] J. O'Reilly, P. Lane, J. Lightwave Technol. 12 (1994) 369.
[4] U. Gliese, S. Norskov, T.N. Nielsen, IEEE Trans. Microwave Theory Tech. 44 (1996) 1716.
[5] G.H. Smith, D. Novak, Z. Ahmed, IEEE Trans. Microwave Theory Tech. 45 (1997) 1410.
[6] C. Lim, A. Nirmalathas, D. Novak, R. Waterhouse, G. Yoffe, J. Lightwave Technol. 18 (2000) 1355.
[7] D. Wake, C.R. Lima, P.A. Davies, IEEE Photon. Technol. Lett. 8 (1996) 578.
[8] U. Gliese, Opt. Quantunm Electron. 30 (1998) 1005.
[9] L.A. Johansson, A.J. Seeds, J. Lightwave Technol. 21 (2003) 511.

[10] T.B. Simpson, F. Doft, IEEE Photon. Technol. Lett. 11 (1999) 1476.
[11] S.C. Chan, J.M. Liu, IEEE J. Sel. Top. Quantum Electron. 10 (2004) 1025.
[12] S.C. Chan, S.K. Hwang, J.M. Liu, Opt. Express 15 (2007) 14921.
[13] J.D. Ralston, S. Weisser, I. Esquivias, E.C. Larkins, J. Rosenzweig, P.J. Tasker, J. Fleissner, IEEE J. Quantum Electron. 29 (1993) 1648.
[14] Y. Matsui, H. Murai, S. Arahira, S. Kutsuzawa, Y. Ogawa, IEEE Photon. Technol. Lett. 9 (1997) 25.
[15] K. Vahala, A. Yariv, IEEE J. Quantum Electron. 19 (1983) 1102.
[16] M.T. van Exter, W.A. Hamel, J.P. Woerdman, B.R.P. Zeijlmans, IEEE J. Quantum Electron. 28 (1992) 1470.
[17] T.B. Simpson, J.M. Liu, A. Gavrielides, IEEE J. Quantum Electron. 32 (1996) 1456.
[18] T.B. Simpson, J.M. Liu, A. Gavrielides, IEEE Photon. Technol. Lett. 7 (1995) 709.
[19] T.B. Simpson, J.M. Liu, IEEE Photon. Technol. Lett. 9 (1997) 1322.
[20] S.K. Hwang, J.M. Liu, J.K. White, IEEE Photon. Technol. Lett. 16 (2004) 972.
[21] L. Chrostowski, X. Zhao, C.J. Chang-Hasnain, IEEE Trans. Microw. Theory Tech. 54 (2006) 788.
[22] E.K. Lau, X. Zhao, H.K. Sung, D. Parekh, C.J. Chang-Hasnain, M. Wu, Opt. Express 16 (2008) 6609.
[23] A. Murakami, K. Kawashima, K. Atsuki, IEEE J. Quantum Electron. 39 (2003) 1196.
[24] S.K. Hwang, D.H. Liang, Appl. Phys. Lett. 89 (2006) 061120.
[25] S. Wieczorek, W.W. Chow, L. Chrostowski, C.J. Chang-Hasnain, IEEE J. Quantum Electron. 42 (2006) 552.
[26] E.K. Lau, H.K. Sung, M. Wu, IEEE J. Quantum Electron. 44 (2008) 90.
[27] H.K. Sung, E.K. Lau, M.C. Wu, IEEE Photon. Technol. Lett. 19 (2007) 1005.
[28] A. Ngoma, D. Fortusini, D. Parekh, W. Yang, M. Sauer, S. Benjamin, W. Hofmann, M.C. Amann, C.J. Chang-Hasnain, J. Lightwave Technol. 28 (2010) 2436.
[29] T.T. Pham, H.S. Kim, Y.Y. Won, S.K. Han, J. Lightwave Technol. 27 (2009) 2457.
[30] G. Cossu, M. Presi, E. Ciaramella, Optical double to single sideband modulation converter for radio-over-fiber systems based on injection-locked Fabry–Perot lasers, Proc. OSA CLEO/QELS, , 2010, CThK4.
[31] C. Hong, C. Zhang, M. Li, L. Zhu, L. Li, W. Hu, A. Xu, Z. Chen, IEEE Photon. Technol. Lett. 22 (2010) 462.
[32] T.B. Simpson, J.M. Liu, K.F. Huang, K. Tai, Quantum Semiclass. Opt. 9 (1997) 765.
[33] J.M. Liu, H.F. Chen, X.J. Meng, T.B. Simpson, IEEE Photon. Technol. Lett. 9 (1997) 1325.
[34] S.C. Chan, S.K. Hwang, J.M. Liu, Opt. Lett. 31 (2006) 2254.
[35] S.K. Hwang, J.M. Liu, J.K. White, IEEE J. Select. Topics Quantum Electron. 10 (2004) 974.
[36] S.K. Hwang, J.M. Liu, Opt. Commun. 169 (1999) 167.
[37] S.K. Hwang, J.M. Liu, Opt. Commun. 183 (2000) 195.
[38] S. Wieczorek, B. Krauskopf, T.B. Simpson, D. Lenstra, Physics Reports 416 (2005) 1.
[39] M. Osinski, J. Buus, IEEE J. Quantum Electron. 23 (1987) 9.
[40] T.B. Simpson, J.M. Liu, Opt. Commun. 112 (1994) 43.
[41] S.K. Hwang, J.B. Gao, J.M. Liu, Phys. Rev. E 61 (2000) 5162.
[42] G.J. Meslener, IEEE J. Quantum Electron. 20 (1984) 1208.
[43] R. Adler, Proc. IRE and Waves and Electrons 34 (1946) 351.